Materials Characterization 130 (2017) 64–73

Contents lists available at ScienceDirect

Materials Characterization

journal homepage: www.elsevier.com/locate/matchar

Analysis of tensile deformation behavior of AM2B® advanced high-strength steel using electron back-scattered diffraction technique

Mohsen Askari-Paykani[a], Hamid Reza Shahverdi[a,*], Reza Miresmaeili[a], Hossein Beladi[b]

[a] Department of Materials Engineering, Tarbiat Modares University, P.O. Box 14115-143, Tehran, Iran
[b] Institute for Frontier Materials, Deakin University, Geelong, VIC 3216, Australia

ARTICLE INFO

Keywords:
Austenite
M_2B
Interrupted tensile test
EBSD analysis
Deformation mechanisms

ABSTRACT

The microstructure evolution of a novel advanced high-strength steel (AM2B® = austenite + $(Fe,Cr)_2B$) subjected to room-temperature interrupted uniaxial tensile test was investigated in relation to the mechanical behavior. This steel showed both high ductility and strength, with yield stress of 357 MPa, ultimate tensile strength of 702 MPa, and total elongation as high as 42%. Electron back-scattered diffraction analysis showed that the high formability (29.4 GPa%) of the current steel was mostly due to energy dissipation mechanisms such as (1) formation and rearrangement of geometrically necessary dislocations (GNDs), (2) activation of mechanical nanotwins, (3) grain rotation, and (4) void nucleation and growth. It was found that GND rearrangement mostly occurred in the true strain range of 0.13–0.25, and void nucleation and growth were the most influential mechanisms in the true strain range of 0.25–0.37. Moreover, it was found that the constraint effect of M_2B phases may accelerate softening (grain rotation) and mechanical nanotwinning.

1. Introduction

Studies are currently focusing on developing third-generation advanced high-strength steel (AHSS) to respond to the demands of the automotive industry for reducing automobile weight and fuel consumption and increasing safety and affordability [1]. These studies are aiming to develop AHSSs with ultimate tensile strength (UTS) and total elongation percentage (El.%) of 500–1600 MPa and 25%–50%, respectively, that are less expensive than second-generation AHSSs [1]. Strengthening mechanisms (e.g., grain refinement, microalloying, and severe plastic deformation) remain a pragmatic approach for increasing the strength of existing AHSSs; at the same time, AHSS development based on composition design and supplementary procedures such as hot rolling, cold rolling, and heat-treatment are also attracting attention [1–9]. Various deformation mechanisms have different effects on mechanical properties. Therefore, understanding the deformation characteristics of newly developed AHSSs will be useful for optimizing the mechanical properties of these steels.

Li et al. [6,8] used in-situ electron back-scattered diffraction (EBSD) to investigate the tensile deformation behavior of the retained austenite in a low-carbon quenching and partitioning steel. Their results showed that the retained austenite at triple edges and twinned austenite transform to martensite with increasing strain. Furthermore, the retained austenite distributed among the martensite undergoes grain rotation along a specific slip plane and direction. Furthermore, they found that the strain distribution is preferentially localized near the martensite/austenite phase boundaries and in the interior of the martensite. Recently, Zhou et al. [9] studied the correlation between toughness mechanisms and microstructures obtained by different heat-treatment processes in S500Q-Z35 steel. Through an EBSD study, they found that owing to larger misorientation boundaries and finer equivalent grain sizes, the mixed microstructure of martensite and lath bainite showed an excellent combination of toughness and strength. Saeidi et al. [10,11] investigated the micromechanisms involved in the high deformation ability of commercial dual-phase 780 (DP780) steel through an EBSD study. They found that grain rotation, void creation and evolution, substructure formation, and stretching of the martensite during deformation were responsible for the high deformation ability of the DP steel. Sun et al. [12] used EBSD to investigate the effect of partitioning time on the relationship between microstructures and mechanical properties in a quenching and partitioning steel. They found that plastic deformation preferentially occurred near the ferrite/martensite interface and then spread to the interior of the ferrite grains with increasing strain. Furthermore, at large plastic deformation, martensite deformation as well as grain rotation and subgrain formation of austenite occur. Eskandari et al. [13] used EBSD to investigate the orientation dependence of the martensitic transformation in a newly developed austenitic lightweight steel. They found that twin-

* Corresponding author at: Jalal e ale Ahmad Hw., Tarbiat Modares University, P.O. Box 14115-143, Tehran, Iran.
E-mail address: shahverdi@modares.ac.ir (H.R. Shahverdi).

http://dx.doi.org/10.1016/j.matchar.2017.05.033
Received 4 March 2017; Received in revised form 14 May 2017; Accepted 26 May 2017
Available online 29 May 2017

assisted martensitic transformation occurred in the ⟨111⟩ ∥TD (tensile direction) orientated austenite grains followed by the twin boundary directly moving to an austenite/martensite phase boundary. Ghasri-Khouzani and McDermid [14] used EBSD to study the critical damage mechanism in Fe-22Mn-XC (X = 0, 0.2, 0.4, and 0.6%) steels. They showed that void formation at matrix/inclusion and austenite/ε-martensite boundaries and void nucleation at grain and matrix/inclusion boundaries led to brittle and ductile fracture in 0C and 0.2C as well as 0.4C and 0.6C steels, respectively. Granados and Rodriguez [15] conducted an EBSD study and found that different cooling rates have a significant effect on the crystal orientation, internal misorientation, and formed substructures in high-strength hot-rolled steel plates and that these changes may affect the mechanical properties of the steel. Recently, Abedi et al. [16] studied the microstructure evolution of a duplex low-density steel with high stacking fault energy (SFE) through interrupted room-temperature tensile tests. Their EBSD results showed that despite the high SFE, substructure evolution provides local areas holding a preferred orientation for twin nucleation.

More recently, using a different strengthening approach based on grain size-, solid solution-, precipitation- and second hard-phase-strengthening mechanisms, we developed and introduced novel kinds of AHSSs in FeCrNiBSi alloy system [2–5]. We added up to 2 wt% boron in an austenitic FeCrNiSi AHSS, which increased both YS and UTS and decreased El.%. These mechanical properties were ascribed to the strain incompatibility of hard M_2B (M = Fe,Cr) phases which formed during casting process and austenitic matrix grains. However, we have not performed a systematic study to address the deformation mechanisms of our developed AHSSs. Since various deformation mechanisms have different effects on mechanical properties, therefore, understanding the deformation characteristics of newly developed AHSSs will be useful for optimizing the mechanical properties of these steels. So considering the superior mechanical properties of novel AM2B® AHSSs [2–5], the present study aims to investigate the room-temperature uniaxial tensile behavior of heat-treated (1100 °C/2 h + 700 °C/2 h) AM2B® AHSS using EBSD, angle-selected backscattered field-emission scanning electron microscopy (AsB-FESEM), and X-ray diffraction (XRD) analysis to clarify the mechanisms behind the high formability of novel AM2B® AHSS.

2. Materials and Methods

Heat-treated (1100 °C/2 h + 700 °C/2 h) hot-rolled AM2B® ($Fe_{65.4}Cr_{15.5}Ni_{14.1}B_{2.0}Si_{3.0}$ (wt%)) AHSS [2–5] sheets with 1-mm thickness were used in this study. Details about the design methodology, material casting route (fast cooling technique), and supplementary processes can be found elsewhere [2–4]. Scanning electron microscopy showed that the initial microstructure consisted of austenite (80 vol%) and M_2B (20 vol%) phases (M = (Fe,Cr)).

By using electrical discharge machining, tensile specimens were cut out of the sheet parallel to the rolling direction (RD). The gauge length and width were 11.4 mm and 3 mm, respectively. By using an Instron tensile testing machine, room-temperature uniaxial tensile tests were conducted at a strain rate of $8.5 \times 10^{-4}\,s^{-1}$ (0.6 mm/min). Four tensile specimens were strained with true strains of 0.05, 0.13, 0.25, and 0.37 (fracture).

The undeformed and deformed microstructures of the specimens were characterized in the rolling direction-normal direction (RD-ND) plane by a FESEM (FEI QUANTA 3D FEG FIB-SEM) equipped with an EBSD detector. The specimens for EBSD analysis were prepared using standard grinding procedures followed by final polishing with a polishing agent consisting of 10 mL 30% concentration hydrogen peroxide and 50 mL colloidal silica. High-resolution EBSD scans were performed with 50-nm beam step size on an area of $78 \times 78\ \mu m^2$. The working distance and operating voltage were 10 mm and 20 kV, respectively. EBSD data was post-processed using a Channel 5 EBSD system (HKL program), and data acquisition was performed using a TSL system. The image quality (IQ), inverse pole figure (IPF), Taylor factor (TF), grain boundary (GB), and Kernel average misorientation (KAM) maps were investigated by EBSD analysis. TF was calculated using cubic symmetry parallel to the tensile loading direction (RD) for FCC active slip systems of {111} ⟨1$\bar{1}$0⟩. KAM maps were obtained, and the 5° average misorientation for a pixel with its five neighbors (5 × 5) was defined. It is reported that the appropriate choice of step size, Kernel size and exclusion angle size (average misorientation criterion) are coupled parameters [17]. As the existence of subgrain is evident in the smallest scan step size, a 50 nm step size was chosen. It is also well known that using a large exclusion angle resulted in calculating on grain boundaries as opposed to the local orientation perturbations [17], so a 5° average misorientation (low angle boundaries criterion) was used. The Kernel size effects essentially mimic the step size effect and as a small step size (50 nm) was used in the current work, a 5 neighbor criteria was also selected. For IQ map, the Kikuchi pattern indexing rate decreased from 95% for the undeformed to 75% for the fractured specimen and all the IQ maps were obtained in the same IQ scale range of 20–300.

3. Results

Fig. 1 shows the engineering and true tensile flow curves as well as the work-hardening rate ($d\sigma/d\varepsilon$, where σ and ε are the true stress and strain, respectively) curve of AM2B® AHSS. The arrows in Fig. 1b indicate the strain levels at which the interrupted uniaxial tensile tests

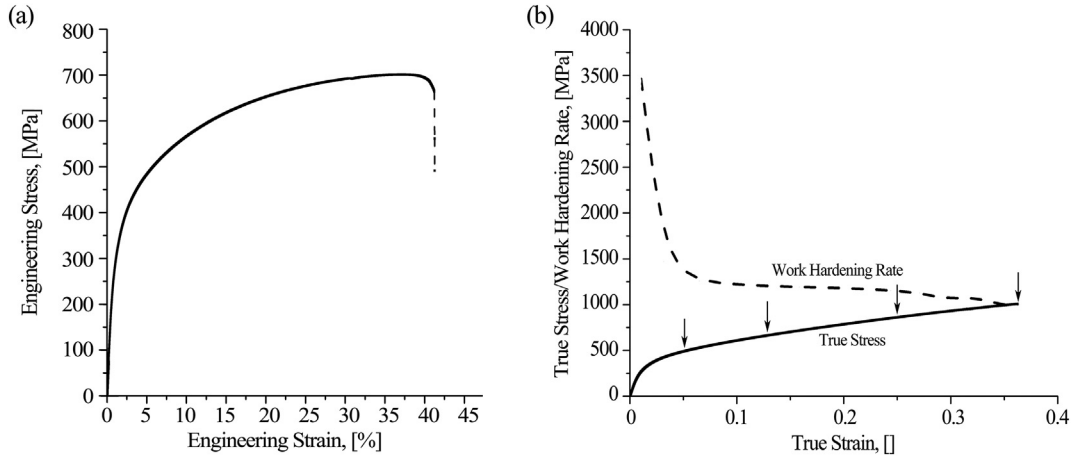

Fig. 1. Engineering stress-strain curve (a) and true stress-strain as well as work hardening rate curves of the AM2B® AHSS (b). Arrows indicate true strains at which interrupted uniaxial tensile tests were performed.